Construction and Validation of a RET TK Catalytic Domain by Homology Modeling†

Tiziano Tuccinardi,‡ Fabrizio Manetti,§ Silvia Schenone,|| Adriano Martinelli,‡ and Maurizio Botta*,§

Dipartimento di Scienze Farmaceutiche, Università di Pisa, via Bonanno 6, I-56126 Pisa, Italy, Dipartimento Farmaco Chimico Tecnologico, Università degli Studi di Siena, Via De Gasperi 2, I-53100 Siena, Italy, and Dipartimento di Scienze Farmaceutiche, Università degli Studi di Genova, Viale Benedetto XV 3, I-16132 Genova, Italy

Received October 11, 2006

RET tyrosine kinase (TK) oncoproteins are potential targets for anticancer therapy. However, the search for novel RET inhibitors has been hampered by the lack of a 3D structure of the receptor. In this study, the "open" and the "closed" structure of the RET TK catalytic domain have been built by homology modeling techniques. The structures were validated by extensive docking studies with practically all the inhibitors reported in the literature and through molecular dynamics simulations of the resulting complexes. All the expected major interactions between the active domain amino acids and the inhibitors have been reproduced in their details. Furthermore, the proposed 3D models are in agreement with the results of available mutation studies. Therefore, these models could be profitably used to filter off from large libraries new potential hit compounds able to target this enzyme.

INTRODUCTION

Carcinomas are in most cases associated with chemical modification of DNA.[1] These modifications can be produced by photochemical reactions, viruses, and reactions induced by chemicals, and a significant number of carcinomas are believed to originate from environmental factors. Polyaromatic hydrocarbons, for example, are exogenous procarcinogens that are metabolized to carcinogenic substances (termed ultimate carcinogens) that react with DNA.[2,3]

With regards to the endogenous carcinogens, they are mainly constituted by hormones and their metabolites.[4]

Oncogenes are altered versions of genes implied in cellular growth and division. The RET proto-oncogene encodes for a transmembrane tyrosine kinase acting as the receptor for growth factors of the glial-derived neurotrophic factor (GDNF) family, including GDNF, neurturin, artemin, and persephin.[5−7] The RET extracellular portion consists of four cadherin-like repeats, a calcium binding site, and a cysteine-rich domain, whereas the intracellular portion contains a tyrosine kinase domain and at least 12 autophosphorylation sites.[8] Ligand-induced dimerization juxtaposes the two catalytic domains, thereby allowing mutual transphosphorylation of tyrosine residues. Phosphotyrosines propagate the signal by recruiting intracellular proteins.

The GDNF-RET signalling pathway plays an important role in survival and differentiation of various neurons as well as in kidney organogenesis.[9,10] Normally, receptor tyrosine kinases (RTK) are tightly regulated, and, when they are deregulated, they become potent oncoproteins.[11] RET mutant forms are responsible for the development of different kinds of cancer: papillary thyroid carcinoma (PTC), the inherited cancer syndrome multiple endocrine neoplasia types 2A and 2B (MEN2A and MEN2B), familial medullary thyroid carcinoma (FMTC), and Hirchsprung disease.[12] The majority of MEN2A and FMTC mutations affect one cysteine residue of the extracellular cysteine-rich RET domain, whereas less frequently, FMTC is associated with changes in the N-terminal (E768D, L790F, Y791F, V804L, V804M) or C-terminal (S891A) lobe of the RET kinase. Most MEN2B and sporadic MTC cases are caused by the M918T mutation in the RET tyrosine kinase domain, while mutations of E768, V804, and M918 are frequently found in sporadic MTCs.[13,14] RET/PTC and RET MEN2A oncoproteins display constitutive kinase activity because of ligand-independent dimerization through the formation of intermolecular disulphide bonds.[15,16] Small molecules, acting as tyrosine kinase (TK) inhibitors, constitute an important class of anticancer agents. They compete with ATP, thereby obstructing autophosphorylation and signal transduction downstream of the target kinase. The search for novel RET kinase inhibitors has been hampered by the lack of an experimental three-dimensional structure of the receptor. However, tyrosine kinases show an extensive conservation of their catalytic domain,[17] which opens the road to homology modeling studies, an approach that, quite surprisingly, has not been yet applied to this receptor.[18] A homology modeling of the catalytic site of the RET kinase is reported in this work. The model was built using two tyrosine kinase receptors as templates. The resulting models were validated through the docking of RET inhibitors.

RESULTS AND DISCUSSION

Homology Modeling. From a computational point of view, kinases represent a very difficult challenge: generally,

* Corresponding author phone: +39 0577 234306; fax: +39 0577 234333; e-mail: botta@unisi.it.

† Taken in part from Dario Iengo, Degree Thesis, Università degli Studi di Siena, 2006.

‡ Università di Pisa.

§ Università degli Studi di Siena.

|| Università degli Studi di Genova.

10.1021/ci6004383 CCC: $37.00
Published on Web 02/13/2007

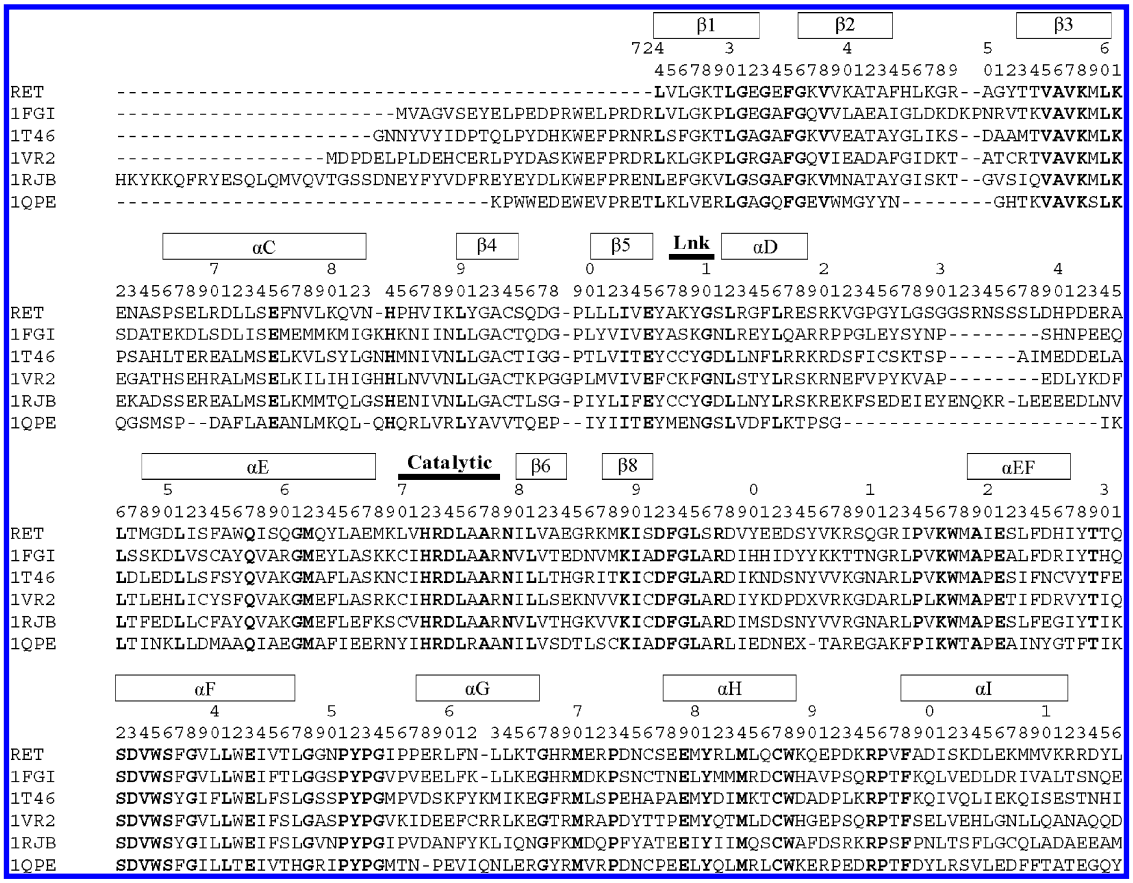

Figure 1. Alignment of RET kinase with the fibroblast growth factor receptor I (1FGI), c-Kit (1T46), vascular endothelial growth factor receptor II (1VR2), FL cytokine receptor (1RJB), and the lymphocyte-specific kinase (1QPE). Conserved residues are in bold. The positions of secondary structure elements are indicated with rectangles, and the catalytic and linker (Lnk) regions are also indicated. In the first line of the alignment scheme, the numeration of RET kinase is reported.

their structures present a wide range of side-chain motion in the ATP binding site, flexible loops, and domain motion between the N and C terminal domains. Moreover, the binding site conformation of these proteins seems to be influenced by the ligand molecular structures, as it can be appreciated by comparing the X-ray structures of the same kinase complexed with different ligands.[19−21]

The search for the best template for modeling was carried out by choosing X-ray structures of kinases possessing a high degree of sequence similarity with RET and complexed with inhibitors structurally similar to known RET inhibitors. The catalytic domain of the FGF tyrosine kinase showed the best sequence similarity with RET (53% of identities, see Figure 1). As a consequence, 1FGI[19] was chosen as the first template. The X-ray structure of the FGF tyrosine kinase has been obtained in complex with its inhibitor SU5402, a substituted indolinone structurally very similar to the strong RET inhibitors compound 3 and compound C (Table 1).[22]

A subsequent extensive analysis of the X-ray structure of complexes between kinases and inhibitors structurally similar to the RET inhibitors[19−21,23] reveals that the binding interaction is greatly influenced by the disposition of the mobile nucleotide-binding loop, the segment between β1 and β2 involved in ATP coordination.

In particular, in the 1FGI structure, as for other inhibitor−kinase complexes,[21] the nucleotide-binding loop undergoes a considerable conformational change upon binding inhibitor (SU5402), placing this loop in contact with the inhibitor and "closing" the ATP-binding site.[19,24]

In order to analyze the mobile nucleotide binding loop disposition, the X-ray structure of kinases showing a nucleotide-binding loop poorly ordered, which leaves the ATP binding site in an "open" state, was also taken into account. Among them, the lymphocyte-specific kinase (1QPE)[20] was chosen as a template for the construction of a second homology model for two main reasons—it displays a good sequence similarity (38% of identity with RET kinase), and its structure has been solved in complex with PP2, which has a high inhibitory activity against RET.[22]

Figure 1 shows the sequence alignment between RET kinase, FGF tyrosine kinase (1FGI),[19] lymphocyte-specific kinase (1QPE),[20] and also three other different type of kinases, namely the c-Kit (1T46),[25] the vascular endothelial growth factor receptor II (1VR2),[26] and the FL cytokine receptor (1RJB),[27] which showed a high degree of sequence similarity with RET.

Following this alignment, two receptor models, representing the "closed" (model 1, obtained from 1FGI) and the "open" state (model 2, obtained from 1QPE) of the enzyme were built and subjected to a simulated annealing protocol by means of the Modeller program.[28] The two best scoring structures were minimized, and their backbone conformations were evaluated by PROCHECK[29] (see Computational section for details). An analysis of the Psi/Phi Ramachandran plot of the resulting proteins indicated that only nine amino acids for model 1 and eight for model 2 had a disallowed geometry (see Figure 2). However, these residues are, in both cases,

Table 1. Compounds Used for the Docking Study

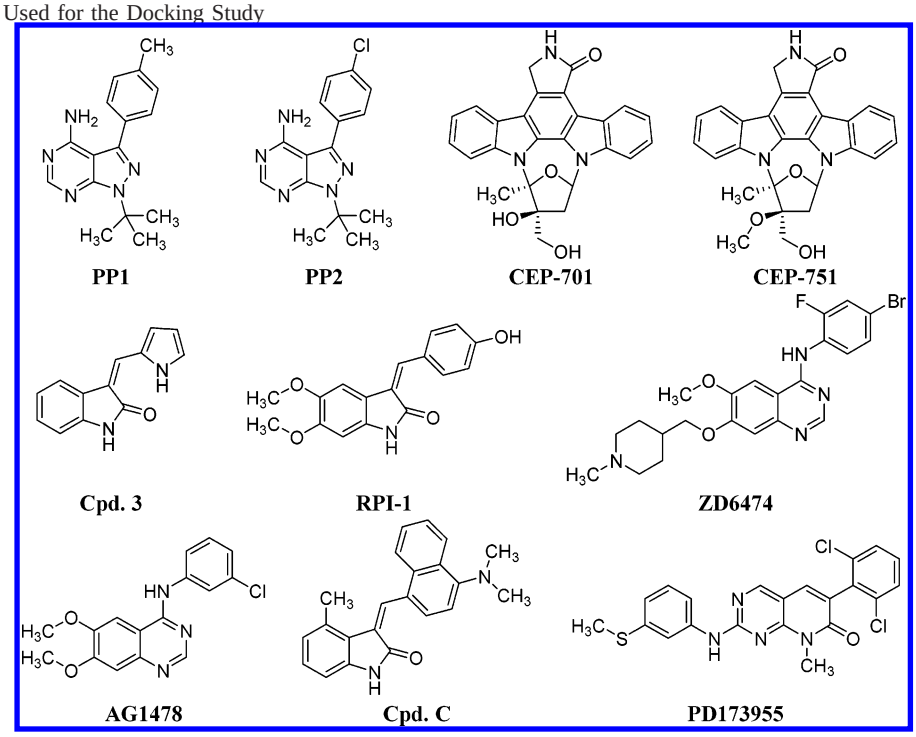

inhibitor	RET inhibition activity (IC_{50}, μM)	inhibitor	RET inhibition activity (IC_{50}, μM)
PP1[22]	0.04[a]	RPI-1[32]	not reported
PP2[29]	0.1[b]	ZD6474[33]	0.1[b]
CEP-701[30]	not reported	AG1478[22]	0.26[a]
CEP-751[30]	not reported	compound C[22]	0.21[a]
compound 3[22]	0.46[a]	PD173955[22]	0.18[a]

[a] Inhibitory activity against recombinant RET kinase. [b] Inhibitory activity against RET/PTC and isolated glutathione-*S*-transferase RET kinase.

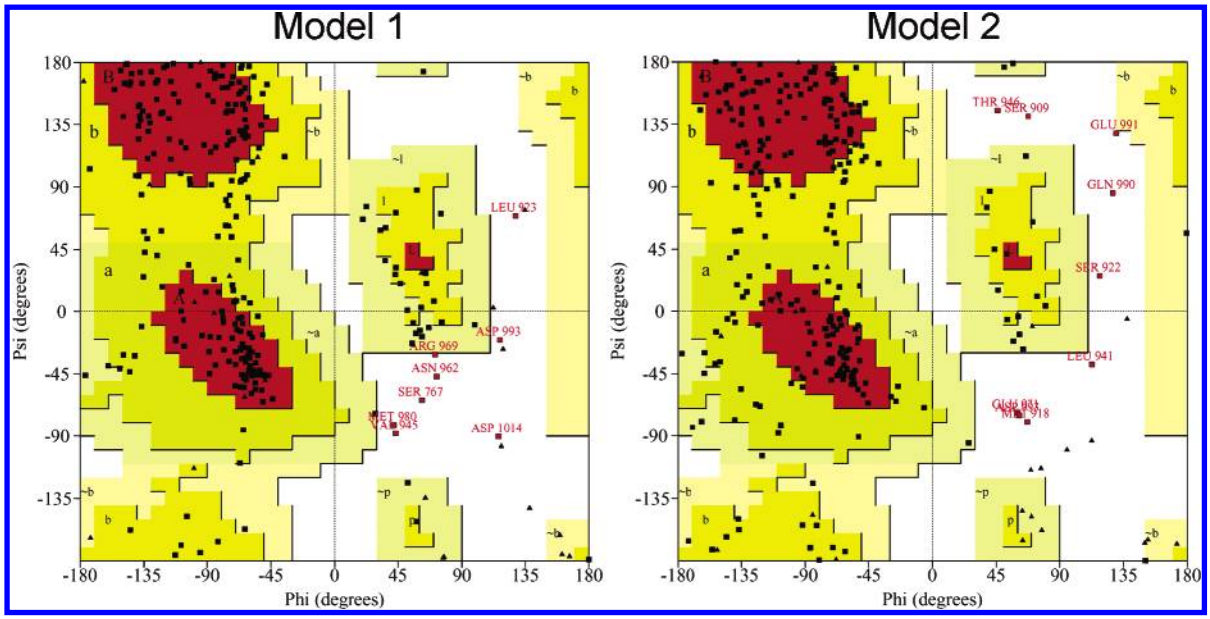

Figure 2. Ramachandran plot of the two models of RET kinase. The most favored regions are colored in red. Allowed, generously allowed, and disallowed regions are indicated as yellow, light yellow, and white regions, respectively. The residues in the disallowed region are marked in red.

far away from the binding site and belong to loops, thereby their influence on the conclusions derived here can be considered negligible.

Obviously, our models have the typical bilobate structure, with the smaller N-terminal domain consisting predominantly of β-sheet structures and the larger C-terminal domain of α-helices that also contains the peptidic substrate binding sites. As shown in Figure 3, the binding sites of the two models mainly differ in the disposition of the nucleotide binding loop, which in model 1 limits the crevice of the

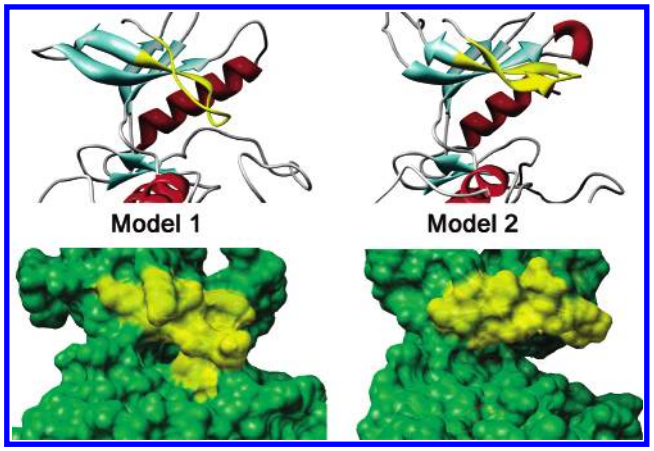

Figure 3. Ribbon diagram and molecular surface of the two models of RET kinase; the nucleotide binding loop is indicated in yellow.

Table 2. Analysis of the Main Interaction of the Ligands Docked into the Two Models[a]

ligand	model 1	model 2
PP1	NO	YES
PP2	NO	YES
ZD6474	NO	YES
RPI-1 (*E*)	NO	NO
RPI-1 (Z)	YES	NO
compound C (E)	NO	NO
compound C (Z)	YES[b]	NO
compound 3	YES	NO
PD173955	YES	YES
AG1478	NO	YES
CEP-701	NO	YES
CEP-751	NO	YES

[a] "YES" is reported if the ligand makes H-bonds with the residues Glu805 and Ala807, otherwise "NO" is reported. [b] The fourth cluster was the first one able to make H-bonds with Glu805 and Ala807.

binding site, whereas in model 2 leaves the binding crevice totally open.

Docking of the Ligands. The reliability of the models was subsequently evaluated by means of docking experiments with practically all the known RET-inhibitors (see Table 1).

All molecules listed in Table 1 were docked within both RET models by means of the AUTODOCK 3.0 program[34] (see Computational section for details).

It is well-known from the analysis of the X-ray complexes between kinases and inhibitors interacting in the ATP binding site[19−21,23] and by pharmacophoric studies[35,36] that the backbone portions of residues 805 and 807 (which correspond to Glu and Ala in RET) play a role in inhibitor binding, as they make hydrogen bonds with N-1 and N-6 of the ATP adenine and also with the most kinase inhibitors.

Consequently, as a first step for validating the docking results, the best docked structure of each ligand into both receptor models was investigated in order to verify if the expected interactions were present.

Interestingly, as shown in Table 2, all the ligands with the exception of PD173955 and compound C, were able to interact with at least one of these two residues in only one of the two receptor models. With regards to PD173955, it was able to interact in both models, whereas the analysis of the docking of compound C (*E* and *Z* configurations) revealed that only the fourth cluster of the *Z* configuration was able to interact with Glu805 and Ala807 in model 1 (this aspect will be discussed below in more detail).

On the basis of the above-mentioned important role of residues Glu805 and Ala807 for the ligand−RET interactions, only complexes in which these interactions were present were taken into account for further analyses. Consequently, for compounds PP1, PP2, ZD6474, AG1478, CEP-701, and CEP-751, the complexes with model 2 were considered, whereas for compounds RPI-1 (*Z* configuration), compound C (the structure of the fourth cluster), and Cpd 3, the complexes with model 1 were considered. In the case of PD173955, both complexes had to be taken into account.

A comparison of the binding mode of some of the considered inhibitors is shown in Figure 4. In the upper part, the general disposition of the ligands in the two models is reported. As examples, docking of compound 3 and PP2 have been considered. In the lower part, the superimposition of the docking results with the X-ray structures are reported.

PP1 and PP2 showed very similar binding modes giving H-bonds with Glu805 and Ala807 through the N5 and 4-amino group, respectively (see Figure 4A). As shown in Figure 4A, the superimposition of the docking result with that coming from the X-ray complex between PP2 and the lymphocyte specific kinase (1QPE) showed a very similar binding mode with a root-mean-square deviation (rmsd) of the ligand position of 1.0 Å, thus confirming our binding hypothesis.

In addition, CEP701 and CEP751 were able to make H-bonds with both Glu805 and Ala807 through the NH and carbonyl of the indol-2-one ring, respectively (see Figure 4B). The results of the docking of these two compounds have been compared with the X-ray complexes between the lymphocyte-specific kinase and a staurosporine structurally very similar to CEP701 and CEP751 (1QPD) and revealed the same binding scheme interaction (see Figure 4B) with a very similar geometry of the ligand into the binding site.

Both AG1478 and ZD6474 were shown to interact with Ala807 forming only one H-bond through the quinazoline ring N1 (see Figure 4C). Furthermore, ZD6474 makes one additional H-bond with Tyr809 through the methylpiperidine ring, thereby stabilizing the ligand binding interaction. Interestingly, Stamos et al. reported the X-ray structure of the EGFR kinase complexed with erlotinib (1M17),[23] possessing the 6,7-disubstituted-quinazoline scaffold similar to AG1478 and ZD6474. The position of erlotinib into the binding site appears to be very similar to that showed by AG1478 and ZD6474 after the docking study (see Figure 4C), in which the H-bond with Met769, corresponding to Ala807 in RET kinase, is maintained.

Differently from the above-described compounds, compound 3 was better allocated in model 1, showing a binding mode very similar to SU5402 complexed with the FGF tyrosine kinase (1FGI).[19]

Furthermore, similarly to this compound, the indol-2-one compound 3 makes two H-bonds with the protein backbone of Glu805 and Ala807 (see Figure 4D).

As far as RPI-1 and compound C are concerned, they are structurally very similar to compound 3, interacting in the same manner but interestingly only in the *Z* configuration. In fact, in this configuration, their aromatic substituent occupies a position similar to that of the pyrrole ring of compound 3 (see Figure 4E).

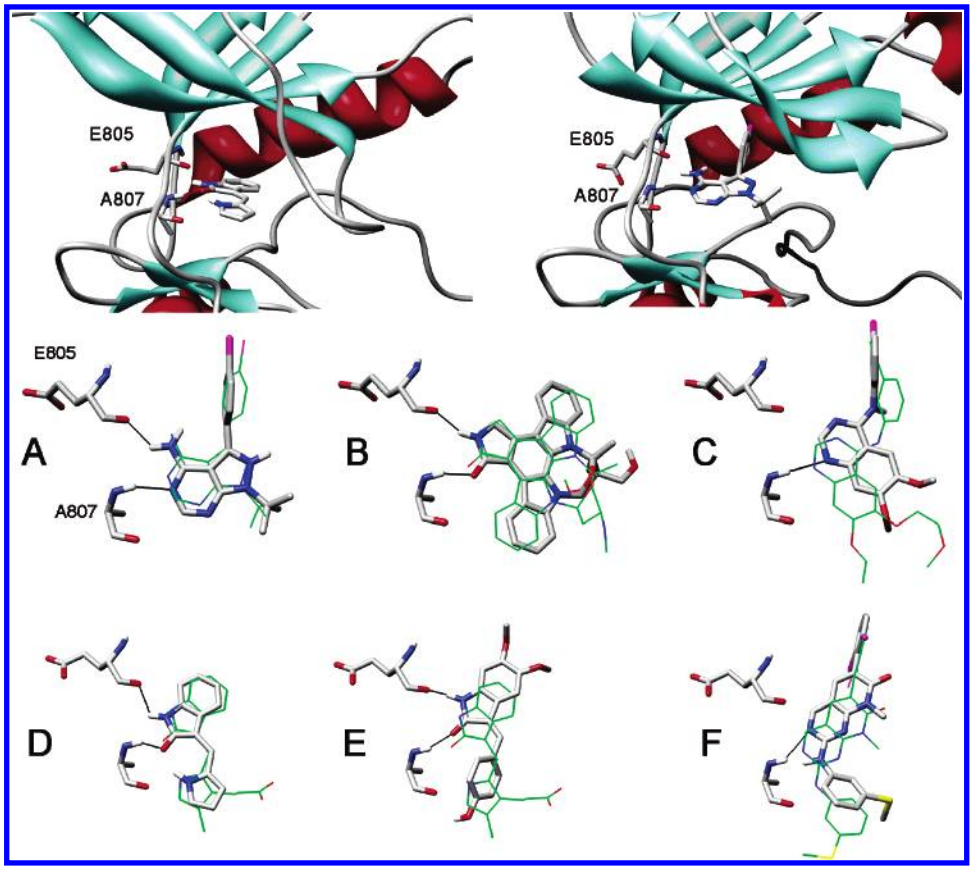

Figure 4. Upper: general disposition of the ligands in the two models (model 1 complexed with compound 3 on the left and model 2 complexed with PP2 on the right). Lower: superimposition between the docking of PP2 and 1QPE, Cep751 and 1QPD, AG1478 and 1M17, compound 3 and 1FGI, RPI-1 and 1FGI, and PD173955 (model 1) and 1M52.

Finally, PD173955 interacts in both receptor models with the same binding mode forming two H-bonds with Ala807 through the pyrido[2,3-*d*]pyrimidine ring N3 and the 2-amino nitrogen (see Figure 4F). This is also confirmed by the superimposition of the docking results with the X-ray of PD173955 complexed with the c-Abl kinase domain (1M52),[21] as the rmsd of the ligand docked in the two models and the crystallized one is 1.8 Å for model 1 and 0.95 Å for model 2.

Molecular Dynamics (MD) Analysis. In order to further validate our models and to perform a more detailed analysis of the ligand−receptor interactions, the above-described RET−inhibitor complexes were subjected to 1 ns of MD simulations.

Results highlighted that all the ligands maintained the interactions with Glu805 and Ala807, as previously suggested by AUTODOCK. In particular, PP1 and PP2 showed a position inside the binding site of model 2 very similar to that suggested by AUTODOCK, with the N5 and 4-amino group of the two ligands linked by H-bonds with Glu805 and Ala807. The 1-*tert*-butyl-1*H*-pyrazolo[3,4-*d*]pyrimidine mainly interacts with Leu881, while the substituted aromatic ring is inserted into a lipophilic pocket formed by Leu779, Ile788, Leu802, and Val804.

Analysis of the MD of Cep701 and Cep751 complexed with model 2 revealed that, beyond the formation of the two H-bonds with Glu805 and Ala807 through the NH and keto oxygen of the lactam ring, they formed a third H-bond with Arg878 through the hydroxymethyl substituent. The lipophilic central core was stabilized by Leu730, Val738, Ile788, and Leu881 (see Figure 5B).

AG1478 maintained the H-bond interaction of the quinazoline ring N1 with Ala807, while the *m*-chlorophenyl substituent was inserted, as the PP1 and PP2 aromatic substituents, into the lipophilic pocket formed by Leu779, I788, Leu802, and Val804.

ZD6474 was described to be more active than AG1478 (see Table 1). Docking studies followed by MD simulations had shown a very similar disposition inside the binding site. However, replacement of the C7 methoxy group with the 1-(methylpiperidin-4-yl)methoxy substituent allowed ZD6474 to form of a second H-bond with the Tyr809 backbone, that, in this case, could be correlated with its higher activity (see Figure 5C).

With regards to the ligands complexed with model 1, after MD simulations, compound 3 showed a binding mode very similar to that suggested by AUTODOCK, maintaining the H-bonds with Glu805 and Ala807 and mainly interacting with Leu730, Phe735, Val738, and Leu881.

Compound C showed a disposition of the indol-2-one central core very similar to that of compound 3; the superimposition between the initial model 1−compound C complex and the final structure after the MD simulation revealed a movement of the nucleotide binding loop, due to the steric not profitable interactions of the *N*, *N*-dimethylnaphthalenamine substituent (see Figure 6). This movement suggests that this compound could interact with a slightly different conformation of the receptor, and this fact could

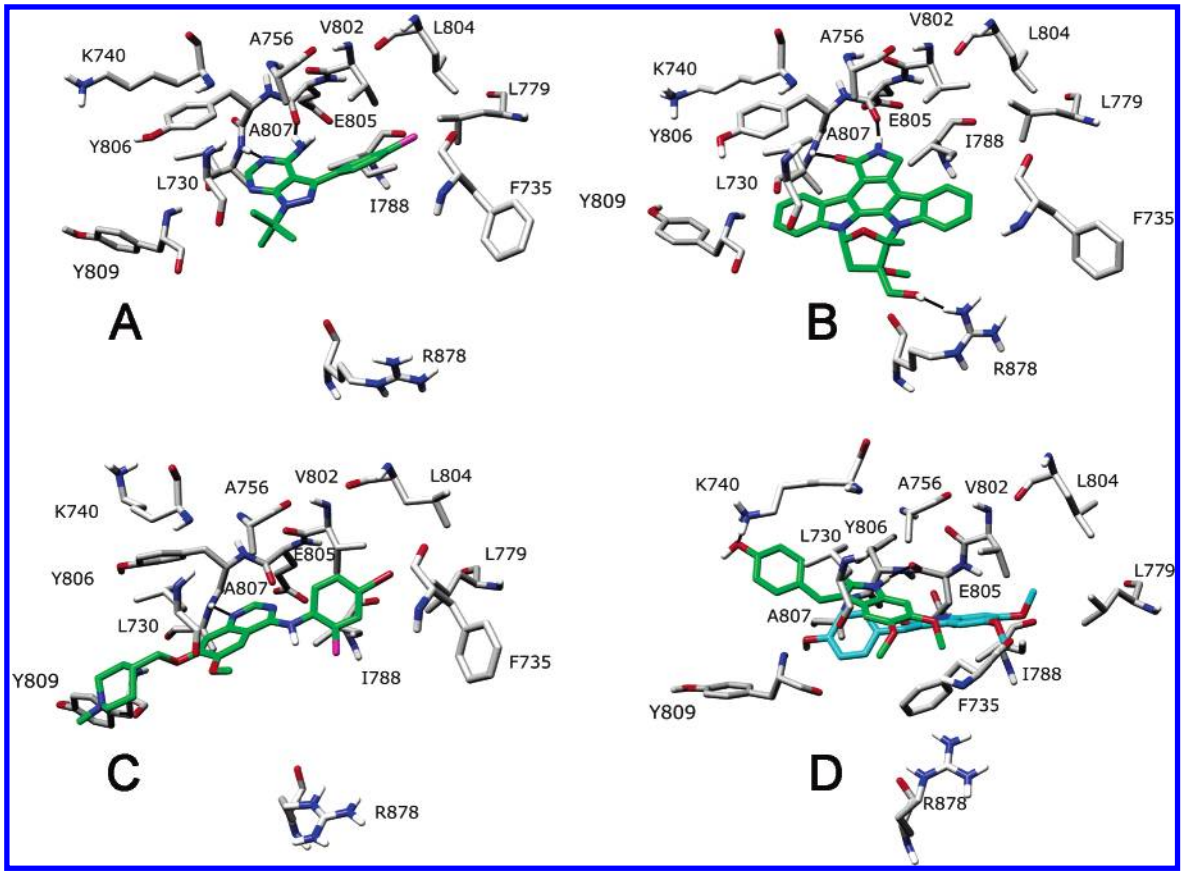

Figure 5. MD simulation results for the complexes of (A) RET with PP2; (B) Cep751; (C) ZD6474; and (D) RPI-1 and its starting disposition (sky blue).

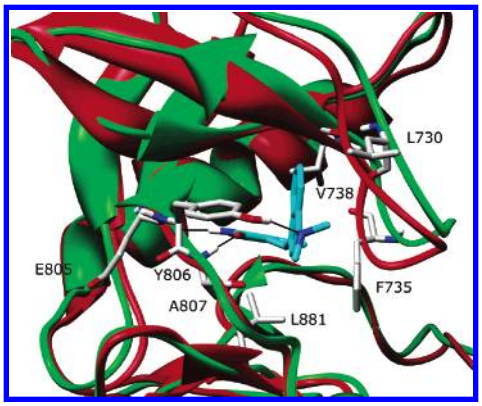

Figure 6. Superimposition between the structure of the RET kinase model 1 used for the automated docking (red) and that obtained after the MD simulation on compound c-RET complex (green).

explain the previously cited problems encountered in the automated docking study of this compound.

Moreover, the 2-fold increase in activity of compound C with respect to compound 3 can be explained by the presence of the *N*, *N*-dimethylnaphthalenamine, which allows a better lipophilic interaction with Leu730 and Val738 and also forms a H-bond with Tyr806 (see Figure 5C).

RPI-1 is the only ligand that during the MD simulation significantly changed its position inside the binding domain. As shown in Figure 5D, RPI-1 was translated about 4.5 Å toward the entrance of the binding site. This shift was probably due to the formation of a H-bond between Lys740 and the phenol hydroxy group. However, the key interactions with Glu805 and Ala807 were still maintained, and, in addition, its dimethoxyindolinone system was well stabilized by the lipophilic interactions with Leu730, Phe735, Val738, Ala756, and Leu881 (see Figure 5D).

Finally, as shown in Figure 7, PD173955 displayed a very similar binding mode in both receptor models. In both models, the ligand formed two H-bonds with Ala807 through the pyrido[2,3-*d*]pyrimidine ring N1 and the 2-amino nitrogen, the *m*-methylthiophenyl substituent was stabilized by lipophilic interactions with Leu730 and Tyr806, and the dichlorophenyl group was inserted into the lipophilic pocket constituted by Leu779, Ile788, and Val804. Its central lipophilic core interacted with Val738, Ala756, and Leu881 and, only in model 1, showed an additional interaction with the Phe735 residue of the nucleotide binding loop (see Figure 7). This suggests that this ligand should prefer the closed form of the receptor (model 1), in agreement with the X-ray structure of PD17395 complexed with the c-Abl kinase domain ("closed" form),[21] in which its nucleotide binding loop assumes a position very similar to that observed in our model 1.

Binding Site Analysis. The catalytic domain of the FGF and the lymphocyte-specific kinase possess a good sequence similarity with RET (53% and 38% of identity, respectively). Furthermore, the RET and FGF tyrosine kinase inhibitors show structural similarity with each other, and PP2, the ligand of the 1QPE structure, is also active against RET.

These data clearly suggest a high binding site similarity between RET and the two kinases used as templates. In order to verify this hypothesis and also to investigate the presence of nonconserved residues in the RET binding site, the two X-ray structures (1FGI and 1QPE) were aligned with model 1 and model 2 of RET complexed with PD173955, and the

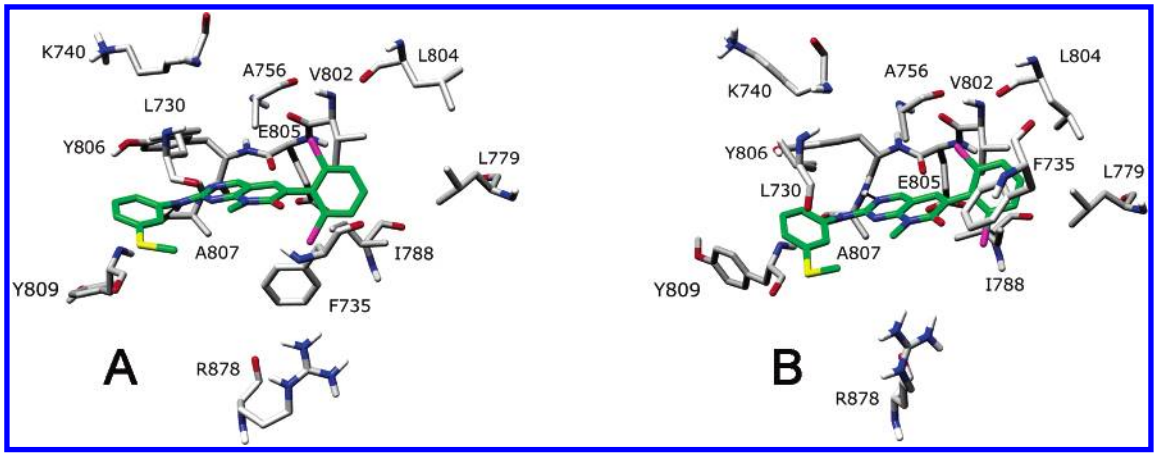

Figure 7. MD simulation results of PD173955 complexed with model 1 (A) and model 2 (B).

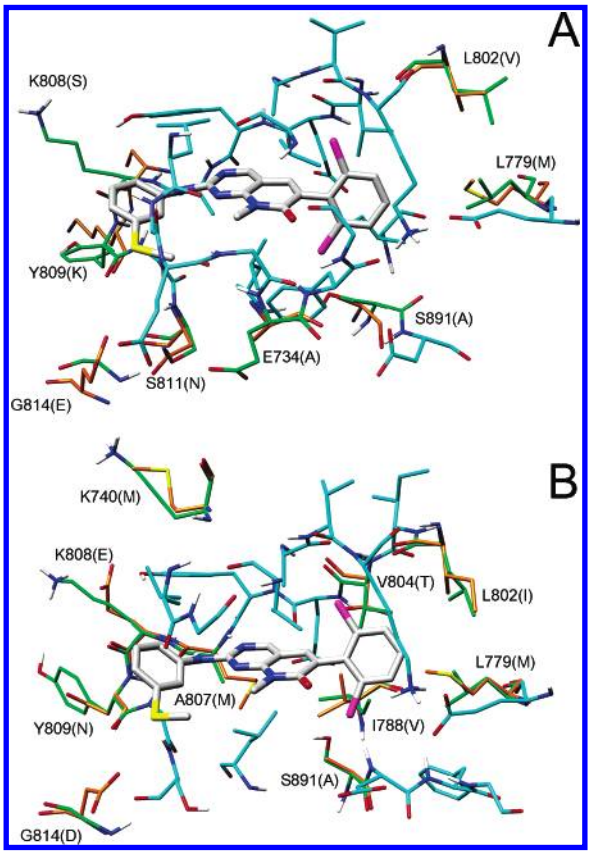

Figure 8. Binding site of model 1 (A) and model 2 (B) complexed with PD173955. The nonconserved residues with respect to 1FGI for model 1 and 1QPE for model 2 are reported in green; the corresponding residues of 1FGI (A) and 1QPE (B) are reported in orange.

binding sites were then analyzed (see Computational section for details).

Figure 8 shows the superimposition between the binding site of model 1 and model 2 for RET and 1FGI and 1QPE X-ray structures.

The RET binding site shows sequence identities of 70% and 62% with the FGF and the lymphocyte-specific kinase, respectively, thus confirming their similarity.

However, this analysis also highlighted the main regions of RET important for binding selectivity. As shown in Figure 8, there are six common nonconserved residues in both 1FGI and 1QPE structures. Among them, Ser891, which is in proximity of the region of interaction of the dichlorophenyl group of PD173955, could be very important since it is substituted by Ala in both 1FGI and 1QPE.

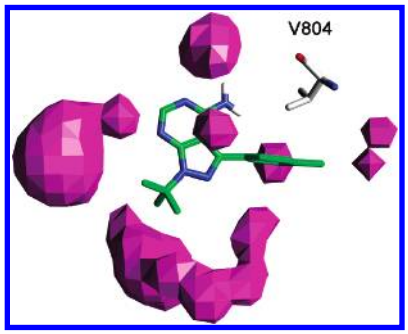

Figure 9. Cavities (violet) around the PP2 and RET kinase binding sites.

With regards to the lipophilic pocket in which the dichlorophenyl group is inserted, Leu779 is not conserved, and it is substituted by Met in both 1FGI and 1QPE. Moreover, in the region of interaction of the *m*-methylthiophenyl substituent of PD173955, Gly814 is substituted in both 1FGI and 1QPE by a charged residue (glutamate and aspartate, respectively).

Mutation Analysis. Recently, Carlomagno et al. demonstrated that the mutation of Val804 with leucine and methionine in the RET kinase domain causes resistance to the three inhibitors PP1, PP2, and ZD6474.[37]

In our RET models, this residue appeared to be fundamental, as it interacts with aromatic substituents of all the three ligands. Furthermore, as shown in Figure 9, the volume of the cavities between the receptor and the ligands reveals that there is no free space in the region around Val804. Therefore, the replacement of Val804 with bulkier residues was expected to induce a loss of activity because of steric hindrance between the ligands and the residues of the binding site.

Following this hypothesis, Val804 of the model 2 RET kinase was mutated with Leu and Met, respectively, and PP1, PP2, and ZD6474 were docked into the two mutated receptors (see Computational section for details). The docking results revealed that the three ligands were unable to interact in the same manner in the mutated model with respect to the model of the wild type protein. In particular, they lost the fundamental interactions with Glu805 and Ala807, in complete agreement with the mutation studies by Carlomagno.[37]

Table 3. Inhibitory Activity at a Concentration of 10 μM of the Screened Compounds with Respect to Staurosporine[a]

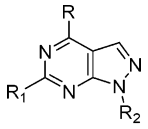

SI

compd	R	R^1	R^2	% inhibition of control values
SI13	$NHCH_2C_6H_5$	H	$CH_2CHClC_6H_5$	25
SI31	$NHCH_2C_6H_4$-*m*Cl	H	$CH_2CHClC_6H_4$-pCl	20
SI47	NHC_4H_9	H	$CH_2CHBrC_6H_5$	18
SI48	$NH(CH_2)_2OC_2H_5$	H	$CH_2CHBrC_6H_5$	10
SI101	NHC_6H_4-*m*Cl	SC_3H_7	$CH_2CHClC_6H_5$	47
SI104	NHC_6H_4-*m*Cl	H	$CH_2CHClC_6H_4$-pF	11
SI109	NHC_3H_7	SCH2CH2-4mph	$CH_2CHClC_6H_5$	48
SI110	$NHCH_2C_6H_5$	SCH2CH2-4mph	$CH_2CHClC_6H_5$	49
SI111	NHC_6H_4-*m*Cl	SCH_3	$CHCHC_6H_5$	71
SI113	$NHCH_2CH_2C_6H_5$	$NHCH_2CH_2OH$	$CHCHC_6H_5$	52

[a] "mph" indicates the morpholinic substituent.

Screening of a Focused Library. As a further study, we screened a focused library of 170 putative kinase inhibitors of general structure SI (see Table 3) already prepared in our laboratory, and some of them have been reported in the literature.[38]

From the docking analysis (see Computational section) on both models, ten compounds were chosen and tested against RET using the Homogeneous Time-Resolved Fluorescence (HTRF) method and staurosporine as a reference kinase inhibitor.[39,40]

Interestingly, the biological data highlighted an inhibitory activity at a concentration of 10 μM ranging from 10 to 71% with respect to staurosporine.

All the compounds that possess a R^1 substituent showed a better RET inhibitory affinity. Figure 10A shows the docking of compound SI111 into model 2. It interacted into the binding site of RET forming a H-bond with A807. The styryl substituent was stabilized by lipophilic interactions with Leu730 and Tyr806, the *m*-chlorophenyl group was inserted into the lipophilic pocket constituted by Leu779, Ile788, Leu802, and Val804, and the thiomethyl substituent was stabilized by the interaction with V738. This binding disposition was very similar to that hypothesized for ZD6474, the styryl substituent simulated the 1-(methylpiperidin-4-yl)-methoxy substituent of ZD6474, the *m*-chlorophenyl group was in a similar disposition of the disubstituted phenyl ring, both ligands formed a H-bond with A807, and finally the thiomethyl group of compound SI111 was near the region of interaction of the metoxy substituent of ZD6474.

The absence of the R^1 substituent determined the inversion of the binding disposition. Figure 10B shows the docking of compound SI13. It exhibited two H-bonds with A807 and the benzyl group interacted with Leu730 and Tyr806, but the chloroethylphenyl substituent did not show any important interaction.

MM_PBSA Analysis. In order to make a more precise analysis of the ligand−protein interactions, the MD trajectories were further analyzed through the MM-PBSA method[41] that has shown to accurately estimate the ligand−receptor energy interaction.[42−45]

This approach averages contributions of gas-phase energies, solvation free energies, and solute entropies calculated for snapshots of the complex molecule as well as the unbound components, extracted from MD trajectories, according to the procedure fully described in the Computational section.

Compounds PP2 and ZD6474 were not tested with the same assays used for the other compounds. However, as shown in Table 4 and Figure 11, reporting the MM-PBSA results calculated for each ligand versus the experimental free energy of binding, there is a quite good quadratic correlation (R^2=0.65), even if the tested ligands are characterized by similar activity values spanning 1.5 order of magnitude, the minimum value of −8.64 (expressed as −log IC_{50}) being associated with compound CPD3 and the maximum value of −10.09 being associated with compound PP1.

With regards to the new ligands tested in this study, compound SI13 showed a calculated free energy of binding worse than that of compound SI111, in agreement with the experimental data.

Comparison of the HM and X-ray Structure of RET. After our homology modeling studies were terminated, the X-ray structures of human RET in both the phosphorylated (2IVS) and non-phosphorylated (2IVR) form and also cocrystallized with PP1 (2IVT) and ZD6474 (2IVU) were reported at 2.00−2.60 Å resolution.[46] Comparison of the X-ray structures with our homology models of RET offers another independent way of validating our results. The RET kinase models are very close to the X-ray structures: the backbone alignment between our models and 2IVU shows an rmsd of 1.2 Å (model 1) and 1.1 Å (model 2) for residues 724−1012. Furthermore, as shown in Figure 12, the overall secondary structure of the models are very similar to the X-ray structure.

The rmsd between the binding site (30 residues within a radius of 7 Å from ZD6474) of 2IVU and model 2 shows a value of 0.7 Å for the backbone and 1.2 Å for all the heavy atoms, thus strongly confirming the reliability of our model.

With regards to the interaction scheme and the disposition of PP1 and ZD6474, the analysis of the X-ray complexes confirms that ZD6474 forms a H-bond with A807, whereas PP1 forms two H-bonds with E805 and A807. Moreover, the rmsd between the position of the two ligands was 1.2 Å for PP1 and 2.1 Å for ZD6474.

The only noticeable difference between our binding hypotheses and the experimental data concerns the 1-(methylpiperidin-4-yl)methoxy substituent of ZD6474, which does not interact in the X-ray complex with the Tyr809 backbone as we had hypothesized.

Finally, the X-ray results confirmed that these two ligands interact in the open conformation of the receptor without any interaction with the nucleotide binding loop.

CONCLUSIONS

RET proto-oncogen is a very well validated model for experimental studies on cancer;[47] nevertheless the 3D structure of this receptor is still unknown. This makes the design of good RET inhibitors very hard, even if studies in this direction have been accelerating in the past few years.

In this study, we report for the first time an approach for the construction of RET TK homology models, predicting

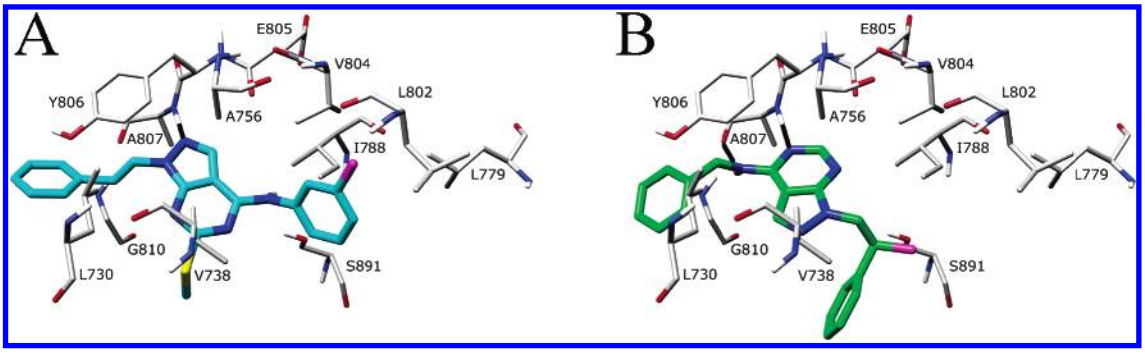

Figure 10. Compound SI111 (on the left) and SI13 (on the right) docked into the RET model 2.

Table 4. Energy Contributions to the Free Energy of Binding (ΔG_{cal}, Expressed as kcal/mol) of Each Compound[a]

compd	IC_{50}, μM	DG_{exp}	ΔE_{MM}	ΔG_{polar}	ΔG_{np}	$-T\Delta S$	ΔG_{cal}	$\Delta\Delta G$
PP1	0.04	−10.09	−46.41	26.23	−5.22	11.68	−13.72	3.63
PP2	0.1	−9.54	−46.01	25.43	−4.96	12.05	−13.49	3.95
compound 3	0.46	−8.64	−51.12	31.68	−3.90	11.01	−12.33	3.69
ZD6474	0.1	−9.54	−59.43	35.88	−6.70	15.93	−14.32	4.78
AG1478	0.26	−8.98	−55.03	34.70	−5.24	12.99	−12.58	3.60
compound C	0.21	−9.10	−59.68	41.20	−5.47	11.52	−12.43	3.33
PD173955_I	0.18	−9.20	−73.80	46.51	−6.53	20.81	−13.01	3.81
PD173955_II	0.18	−9.20	−68.9	41.04	−6.40	21.28	−12.98	3.78
SI13	ND	ND	−46.09	29.98	−5.51	15.26	−6.36	ND
SI111	ND	ND	−58.85	36.84	−5.99	16.54	−11.46	ND

[a] The energy difference ($\Delta\Delta G$) between the calculated (ΔG_{cal}) and the experimental free energy of binding (ΔG_{exp}) was also reported. ND means "not determined". See the Computational section for the other terms. For PD173955, the free energy of binding was calculated in both model 1 (PD173955_I) and model 2 (PD173955_II).

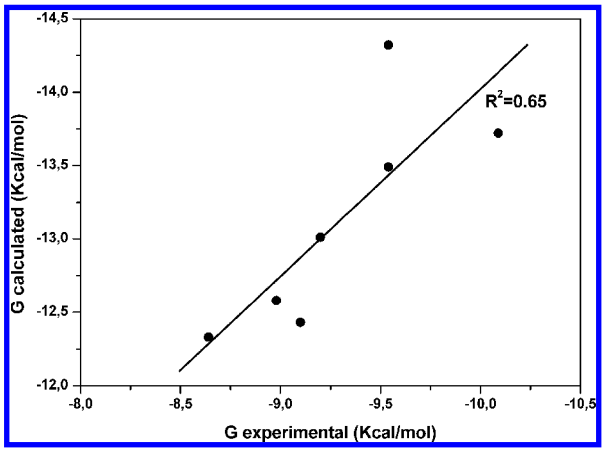

Figure 11. Experimental vs predicted free energy of binding for the analyzed ligands. The values are expressed as kcal/mol.

the structure of the enzyme in both the "open" and "closed" forms. The models agree with reported mutagenesis studies and have been tested using practically all known RET inhibitors and validated through an automated docking/MD simulation method.

All the expected major interactions between the active domain amino acids and the inhibitors could be described in detail.

Furthermore, the models were used to filter a focused library of 170 compounds, obtaining a new potential hit for RET kinase inhibition. A synthetic development will be done to increase the activity of these compounds, investigating in particular the possible interaction with Ser891, which could be a very interesting "anchor-point" for the ligands. Moreover, a larger library screening will be carried out in order to find new active compounds.

COMPUTATIONAL SECTION

Homology Modeling. All the primary sequences were obtained from the SWISS-PROT protein sequence database.[48] Sequence similarity searches were carried out using Blast.[49] The crystal structures of the FGF tyrosine kinase (1FGI)[19] and the lymphocyte-specific kinase (1QPE)[20] were taken from the Brookhaven Protein Data Bank.[50] The sequence alignment of the chosen kinases were performed by CLUSTAL W,[51] with a gap open penalty of 10 and a gap extension penalty of 0.05. The two starting models of the RET kinase were constructed using Modeller.[28] The loop regions comprised between residues A743-Y752 and R820-A845 were constructed by means of the "Loop optimization method" of Modeller, applying the "very_slow" loop refinement method. Starting from these two receptors, ten structures were generated by means of the "very slow MD annealing" refinement method, as implemented in Modeller, and the best two receptor models were chosen on the basis of the Discrete Optimized Protein Energy (DOPE) assessment method and minimized. The backbone conformation of the resulting receptor structures was evaluated by inspection of the Ramachandran plot using PROCHECK.[29] The molecular minimization was carried out through the AMBER 8 program,[52] using the parm94 force field at 300 K. An explicit solvent model TIP3P water was used, and the complexes were solvated with a 10 Å water cap. Chlorine ions were added as counterions to neutralize the system. The protein was then minimized though 5000 steps of Steepest Descent (SD) followed by Conjugate Gradient (CG) until a convergence of 0.05 kcal/Å·mol.

Docking of the Ligands. The X-ray geometry of compounds complexed with kinases were used as a scaffold for the construction of the docked ligands, which were then minimized with Macromodel,[53] using the CG method until

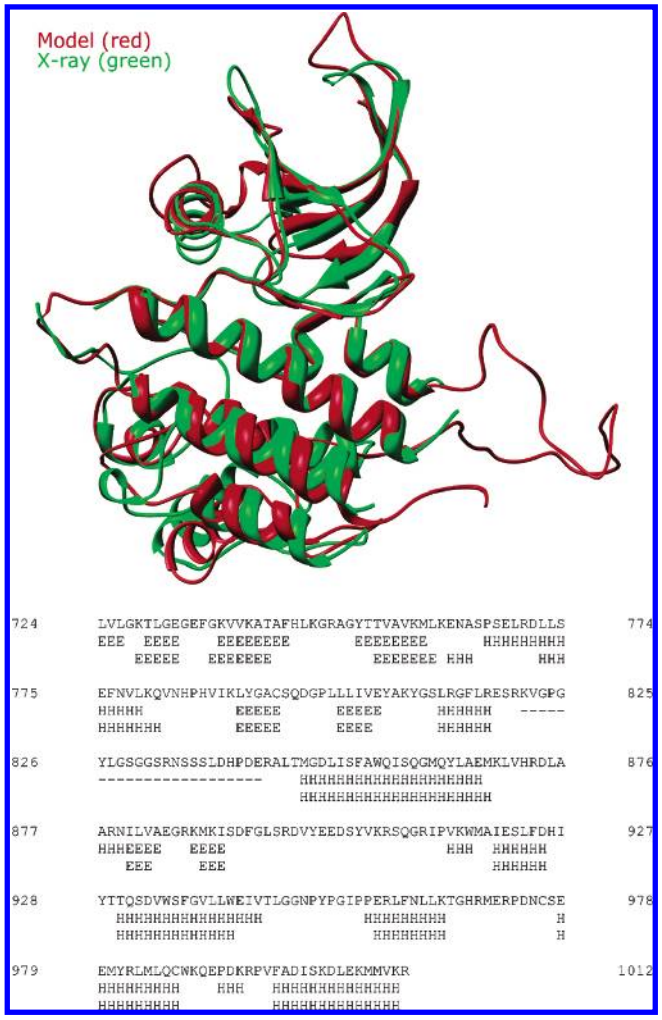

Figure 12. Superimposition between our RET homology model (model 1) and the published X-ray structure. The α-elix and *β*-sheet are indicated with 'H' and 'E', respectively.

a convergence value of 0.05 kcal/Å·mol, with MMFFs as the forcefield and a distance-dependent dielectric constant of 4.0. Both the *Z* and *E* configurations were taken into account for RPI-1 and compound C.

The ligands were docked into the two models using the AUTODOCK 3.0 program.[34] AUTODOCK TOOLS[54] was used to identify the torsion angles in the ligands, add the solvent model, and assign partial atomic charges (Gasteiger for the ligands and Kollman for the receptors). The regions of interest used by AUTODOCK were defined by superimposing model 1 and model 2 to their templates, respectively, and considering the complexed ligands as the central group of a grid of 46, 40, and 48 points in the *x*, *y*, and *z* directions, respectively.

Using the Lamarckian Genetic Algorithm, the compounds were subjected to 100 runs of the AUTODOCK search, with default values for the other parameters.

The RET−inhibitor complexes in which the best docked structure of the ligands made H-bonds with Glu805 and/or Ala807 were then subjected to MD simulations.

MD Simulations. All simulations were performed using AMBER 8.[52] MD simulations were carried out using the same conditions described above for the minimization of the two models.

Prior to MD simulations, two steps of minimization were carried out. In the first stage, we kept the protein fixed with a position restraint of 500 kcal/mol/Å^2, and we just minimized the positions of the water molecules. In the second stage, we minimized the entire system applying a restraint of 50 kcal/mol/Å^2 on the α carbons. The two minimization stages consisted of 5000 steps in which the first 1000 were SD and the last 4000 CG.

MD trajectories were run using the minimized structure as the starting conformation, the time step of the simulations was 2.0 fs with a cutoff of 12 Å for the nonbonded interaction, and SHAKE was employed to keep all bonds involving hydrogen atoms rigid. Constant-volume was carried out for 100 ps, during which the temperature was raised from 0 to 300 K; then 1 ns of constant-pressure MD was carried out at 300 K. For temperature regulation, we used the Langevin thermostat to maintain the temperature of our system at 300 K. This temperature control method is significantly more efficient at equilibrating the system temperature than the Berendsen temperature coupling scheme, and it is the recommended choice in AMBER 8.0.[55−57]

In the first 600 ps of MD, all the α carbons of the receptor were blocked with a harmonic force constant, which was decreased from 10 to 1 kcal/mol/Å^2 during the simulation time. In the last 400 ps of the simulation, the residues in the range of 10 Å from the ligand were left free. The final structure of the complexes was obtained as the average of the last 400 ps of MD minimized with the CG method until a convergence of 0.05 kcal/mol·Å. During the first 200 ps, a distance constraint of 30 kcal/mol/Å^2 was applied on the ligand−receptor interactions that involved Glu805 and Ala807.

General Amber Force Field (GAFF) parameters were assigned to ligands, while partial charges were calculated using the AM1-BCC method as implemented in the Antechamber suite of AMBER 8.

Binding Site Analysis. Using the above-described alignment, the heavy atoms of model 1 and model 2 of RET obtained through the MD simulations in complex with PD173955 were aligned with 1FGI and 1QPE, respectively. The binding sites were then defined including all the residues within a radius of 5 Å from the ligand.

Mutation Analysis. The two models were mutated through the "Mutate task" of Maestro 7.5[53] and minimized as described above. The docking studies were developed using the same grid dimension used for the docking analysis into the two wild receptors.

Library Screening. The compounds of the focused library were docked into both models following the above-described procedure. Compounds able to form (with one of the two RET models) at least one H-bond with the backbone of residues 805 and 807, were selected. They were then visually checked to assess their diversity, and from this analysis ten compounds were tested.

Energy Evaluation. We extracted from the last 400 ps of MD of the ligand−RET complexes, 100 snapshots (at time intervals of 4 ps) for each species (complex, receptor, and ligand). The various MM-PBSA energy terms in eq 1 were computed as follows:

$$G = G_{\text{polar}} + G_{\text{nonpolar}} + E_{\text{mm}} - \text{TS} \qquad (1)$$

Electrostatic, van der Waals, and internal energies (E_{mm}) were obtained using the SANDER module in AMBER 8.0.[52]

Polar energies (G_{polar}) were obtained from the PBSA module of the AMBER 8.0 program (using the Poisson−Boltzmann method) applying dielectric constants of 1 and 80 to represent the gas and water phases, respectively. Nonpolar energies ($G_{nonpolar}$) were determined using the MOLSURF program.

Solute entropy was evaluated in order to correlate the predicted free energy of binding (calculated as in eq 2) with the experimental one. It was estimated using the NMODE module of AMBER 8.0 on a total of 10 snapshots. Prior to the normal mode calculations, each species (complex, receptor, or ligand) was subjected to a CG energy minimization using a distance dependent dielectric, until a convergence of 0.0001 kcal/mol·Å.

$$\Delta G_{bind} = G_{complex} - (G_{protein} + G_{ligand}) \qquad (2)$$

ACKNOWLEDGMENT

Financial support from Fondazione Monte dei Paschi di Siena is gratefully acknowledged. We also thank Prof. Anna Tramontano for her precious support. This manuscript was taken in part from Dario Iengo, Degree Thesis, Università degli Studi di Siena, 2006.

REFERENCES AND NOTES

(1) Kranjc, A.; Mavri, J. Guanine alkylation by ethylene oxide: calculation of chemical reactivity. *J. Phys. Chem. A* **2006**, *110*, 5740−5744.
(2) Volk, D. E.; Rice, J. S.; Luxon, B. A.; Yeh, H. J. C.; Liang, C.; Xie, G.; Sayer, J. M.; Jerina, D. M.; Gorenstein, D. G. NMR evidence for syn-anti interconversion of a trans opened (10*R*)-dA adduct of benzo-[a]pyrene (7*S*, 8*R*)-diol (9*R*, 10*S*)-epoxide in a DNA duplex. *Biochemistry* **2000**, *39*, 14040−14053.
(3) Ramesha, A. R.; Kroth, H.; Jerina, D. M. Solvent-free synthesis of benzo[a]pyrene 7,8-diol 9,10-epoxide adducts at the N(2)-position of deoxyguanosine. *Org. Lett.* **2001**, *3*, 531−533.
(4) Huetz, P.; Kamarulzaman, E. E.; Wahab, H. A.; Mavri, J. Chemical reactivity as a tool to study carcinogenicity: reaction between estradiol and estrone 3,4-quinones ultimate carcinogens and guanine. *J. Chem. Inf. Comput. Sci.* **2004**, *44*, 310−314.
(5) Pachnis, V.; Mankoo, B.; Costantini, F. Expression of the c-ret proto-oncogene during mouse embryogenesis. *Development* **1993**, *119*, 1005−1017.
(6) Trupp, M.; Arenas, E.; Fainzilber, M.; Nilsson, A. S.; Sieber, B. A.; Grigoriou, M.; Kilkenny, C.; Salazar-Grueso, E.; Pachnis, V.; Arumae, U. Functional receptor for GDNF encoded by the c-ret proto-oncogene. *Nature* **1996**, *381*, 785−789.
(7) Buj-Bello, A.; Adu, J.; Pinon, L. G; Horton, A.; Thompson, J.; Rosenthal, A.; Chinchetru, M.; Buchman, V. L.; Davies, A. M. Neurturin responsiveness requires a GPI-linked receptor and the Ret receptor tyrosine kinase. *Nature* **1997**, *387*, 721−724.
(8) Santoro, M.; Melillo, R. M.; Carlomagno, F.; Vecchio, G.; Fusco, A. Minireview: RET: normal and abnormal functions. *Endocrinology* **2004**, *145*, 5448−5451.
(9) Pichel, J. G.; Shen, L.; Sheng, H. Z.; Granholm, A. C.; Drago, J.; Grinberg, A.; Lee, E. J.; Huang, S. P.; Saarma, M.; Hoffer, B. J.; Sariola, H.; Westphal, H. Defects in enteric innervation and kidney development in mice lacking GDNF. *Nature* **1996**, *382*, 73−76.
(10) Sanchez, M. P.; Silos-Santiago, I.; Frisen, J.; He, B.; Lira, S. A.; Barbacid, M. Renal agenesis and the absence of enteric neurons in mice lacking GDNF. *Nature* **1996**, *382*, 70−73.
(11) Futreal, P. A.; Coin, L.; Marshall, M.; Down, T.; Hubbard, T.; Wooster, R.; Rahman, N.; Stratton, M. R. A census of human cancer genes. *Nat. Rev. Cancer* **2004**, *4*, 177−183.
(12) Manie, S.; Santoro, M.; Fusco, A.; Billaud, M. The RET receptor: function in development and dysfunction in congenital malformation. *Trends Genet.* **2001**, *17*, 580−589.
(13) Bolino, A.; Schuffenecker, I.; Luo, Y.; Seri, M.; Silengo, M.; Tocco, T.; Chabrier, G.; Houdent, C.; Murat, A.; Schlumberger, M.; Tourniare, J.; Lenoir, G. M.; Romeo, G. RET mutations in exons 13 and 14 of FMTC patients. *Oncogene* **1995**, *10*, 2415−2419.
(14) Ponder, B. A. The phenotypes associated with ret mutations in the multiple endocrine neoplasia type 2 syndrome. *Cancer Res.* **1999**, *59* (7 Suppl), 1736s−1741s.
(15) Santoro, M.; Carlomagno, F.; Romano, A.; Bottaio, D. P.; Dathan, N. A.; Greco, M.; Fusco, A.; Vecchio, G.; Matoskova, B.; Kraus, M. H.; Di, Fiore, P. P. Activation of RET as a dominant transforming gene by germline mutations of MEN2A and MEN2B. *Science* **1995**, *267*, 381−383.
(16) Monaco, C.; Visconti, R.; Barone, M. V.; Pierantoni, G. M.; Berlingieri, M. T.; De Lorenzo, C.; Mineo, A.; Vecchio, G.; Fusco, A.; Santoro, M. The RFG oligomerization domain mediates kinase activation and re-localization of the RET/PTC3 oncoprotein to the plasma membrane. *Oncogene* **2001**, *20*, 599−608.
(17) Traxler, P.; Furet, P. Strategies toward the design of novel and selective protein tyrosine kinase inhibitors. *Pharmacol. Ther.* **1999**, *82*, 195−206.
(18) In "Plaza Menacho, I.; Koster, R.; van der Sloot, A. M.; Quax, W. J.; Osinga, J.; van der Sluis, T.; Hollema, H.; Burzynski, G. M.; Gimm, O.; Buys, C. H.; Eggen, B. J.; Hofstra, R. M. RET-familial medullary thyroid carcinoma mutants Y791F and S891A activate a Src/JAK/STAT3 pathway, independent of glial cell line-derived neurotrophic factor. *Cancer Res.* **2005**, *65*, 1729−1737." the authors reported a 3D structure of the RET catalytic domain, with the aim of investigating the effects of Y791F and S891A mutations. None of the inhibitors docking study was reported, and neither was information on construction of the catalytic domain.
(19) Mohammadi, M.; McMahon, G.; Sun, L.; Tang, C.; Hirth, P.; Yeh, B. K.; Hubbard, S. R.; Schlessinger, J. Structures of the tyrosine kinase domain of fibroblast growth factor receptor in complex with inhibitors. *Science* **1997**, *276*, 955−960.
(20) Zhu, X.; Kim, J. L.; Newcomb, J. R.; Rose, P. E.; Stover, D. R.; Toledo, L. M.; Zhao, H.; Morgenstern, K. A. Structural analysis of the lymphocyte-specific kinase Lck in complex with non-selective and Src family selective kinase inhibitors. *Struct. Fold. Des.* **1999**, *7*, 651−661.
(21) Nagar, B.; Bornmann, W. G.; Pellicena, P.; Schindler, T.; Veach, D. R.; Miller, W. T.; Clarkson, B.; Kuriyan, J. Crystal structures of the kinase domain of c-Abl in complex with the small molecule inhibitors PD173955 and imatinib (STI-571). *Cancer Res.* **2002**, *62*, 4236−4243.
(22) Mologni, L.; Sala, E.; Riva, B.; Cesaro, L.; Cazzaniga, S.; Redaelli, S.; Marin, O.; Pasquato, N.; Donella-Deana, A.; Gambacorti-Passerini, C. Expression, purification, and inhibition of human RET tyrosine kinase. *Protein Expression Purif.* **2005**, *41*, 177−185.
(23) Stamos, J.; Sliwkowski, M. X.; Eigenbrot, C. Structure of the epidermal growth factor receptor kinase domain alone and in complex with a 4-anilinoquinazoline inhibitor. *J. Biol. Chem.* **2002**, *277*, 46265−46272.
(24) Manetti, F.; Botta, M. Small-molecule inhibitors of fibroblast growth factor receptor (FGFR) tyrosine kinases (TK). *Curr. Pharm. Des.* **2003**, *9*, 567−581.
(25) Mol, C. D.; Dougan, D. R.; Schneider, T. R.; Skene, R. J.; Kraus, M. L.; Scheibe, D. N.; Snell, G. P.; Zou, H.; Sang, B. C.; Wilson, K. P. Structural basis for the autoinhibition and STI-571 inhibition of c-Kit tyrosine kinase. *J. Biol. Chem.* **2004**, *279*, 31655−31663.
(26) McTigue, M. A.; Wickersham, J. A.; Pinko, C.; Showalter, R. E.; Parast, C. V.; Tempczyk-Russell, A.; Gehring, M. R.; Mroczkowski, B.; Kan, C. C.; Villafranca, J. E.; Appelt, K. Crystal structure of the kinase domain of human vascular endothelial growth factor receptor 2: a key enzyme in angiogenesis. *Struct. Fold. Des.* **1999**, *7*, 319−330.
(27) Griffith, J.; Black, J.; Faerman, C.; Swenson, L.; Wynn, M.; Lu, F.; Lippke, J.; Saxena, K. The structural basis for autoinhibition of FLT3 by the juxtamembrane domain. *Mol. Cell* **2004**, *13*, 169−178.
(28) Fiser, A.; Do, R. K.; Sali, A. Modeling of loops in protein structures. *Protein Sci.* **2000**, *9*, 1753−1773.
(29) Laskowski, R. A.; MacArthur, M. W.; Moss, D. S.; Thorton, J. M. PROCHECK: a program to check the stereochemical quality of protein structures. *J. Appl. Crystallogr.* **1993**, *26*, 283−291.
(30) Carlomagno, F.; Vitagliano, D.; Guida, T.; Basolo, F.; Castellone, M. D.; Melillo, R. M.; Fusco, A.; Santoro, M. Efficient inhibition of RET/papillary thyroid carcinoma oncogenic kinases by 4-amino-5-(4-chlorophenyl)-7-(*t*-butyl)pyrazolo[3,4-*d*]pyrimidine (PP2). *J. Clin. Endocrinol. Metab.* **2003**, *88*, 1897−1902.
(31) Strock, C. J.; Park, J. I.; Rosen, M.; Dionne, C.; Ruggeri, B.; Jones-Bolin, S.; Denmeade, S. R.; Ball, D. W.; Nelkin, B. D. CEP-701 and CEP-751 inhibit constitutively activated RET tyrosine kinase activity and block medullary thyroid carcinoma cell growth. *Cancer Res.* **2003**, *63*, 5559−5563.
(32) Lanzi, C.; Cassinelli, G.; Pensa, T.; Cassinis, M.; Gambetta, R. A.; Borrello, M. G.; Menta, E.; Pierotti, M. A.; Zunino, F. Inhibition of transforming activity of the ret/ptc1 oncoprotein by a 2-indolinone derivative. *Int. J. Cancer.* **2000**, *85*, 384−390.
(33) Carlomagno, F.; Vitagliano, D.; Guida, T.; Ciardiello, F.; Tortora, G.; Vecchio, G.; Ryan, A. J.; Fontanini, G.; Fusco, A.; Santoro, M. ZD6474, an orally available inhibitor of KDR tyrosine kinase activity, efficiently blocks oncogenic RET kinases. *Cancer Res.* **2002**, *62*, 7284−7290.

(34) Morris, G. M.; Goodsell, D. S.; Halliday, R. S.; Huey, R.; Hart, W. E.; Belew, R. K.; Olson, A. J. Automated Docking Using a Lamarckian Genetic Algorithm and and Empirical Binding Free Energy Function. *J. Comput. Chem.* **1998**, *19*, 1639−1662.
(35) Traxler, P.; Green, J.; Mett, H.; Sequin, U.; Furet, P. Use of a pharmacophore model for the design of EGFR tyrosine kinase inhibitors: isoflavones and 3-phenyl-4(1*H*)-quinolones. *J. Med. Chem.* **1999**, *42*, 1018−1026.
(36) Traxler, P.; Furet, P. Strategies toward the design of novel and selective protein tyrosine kinase inhibitors. *Pharmacol. Ther.* **1999**, *82*, 195−206.
(37) Carlomagno, F.; Guida, T.; Anaganti, S.; Vecchio, G.; Fusco, A.; Ryan, A. J.; Billaud, M.; Santoro, M. Disease associated mutations at valine 804 in the RET receptor tyrosine kinase confer resistance to selective kinase inhibitors. *Oncogene* **2004**, *23*, 6056−6063.
(38) Schenone, S.; Bruno, O.; Bondavalli, F.; Ranise, A.; Mosti, L.; Menozzi, G.; Fossa, P.; Donnini, S.; Santoro, A.; Ziche, M.; Manetti, F.; Botta, M. Antiproliferative activity of new 1-aryl-4-amino-1*H*-pyrazolo[3,4-*d*]pyrimidine derivatives toward the human epidermoid carcinoma A431 cell line. *Eur. J. Med. Chem.* **2004**, *39*, 939−946.
(39) Cerep drug discovery company. http://www.cerep.fr.
(40) Borrello, M. G.; Alberti, L.; Arighi, E.; Bongarzone, I.; Battistini, C.; Bardelli, A.; Pasini, B.; Piutti, C.; Pizzetti, M. G.; Modellini, P.; Radice, M. T.; Pienotti, M. A. The full oncogenic activity of Ret/ptc2 depends on tyrosine 539, a docking site for phospholipase Cγ. *Mol. Cell. Biol.* **1996**, *16*, 2151−2163.
(41) Kollman, P. A.; Massova, I.; Reyes, C.; Kuhn, B.; Huo, S.; Chong, L.; Lee, M.; Lee, T.; Duan, Y.; Wang, W.; Donini, O.; Cieplak, P.; Srinivasan, J.; Case, D. A.; Cheatham, T. E. 3rd Calculating structures and free energies of complex molecules: combining molecular mechanics and continuum models. *Acc. Chem. Res.* **2000**, *33*, 889−897.
(42) Kuhn, B.; Kollman, P. A. Binding of a diverse set of ligands to avidin and streptavidin: an accurate quantitative prediction of their relative affinities by a combination of molecular mechanics and continuum solvent models. *J. Med. Chem.* **2000**, *43*, 3786−3791.
(43) Donini, O. A.; Kollman, P. A. Calculation and prediction of binding free energies for the matrix metalloproteinases. *J. Med. Chem.* **2000**, *43*, 4180−4188.
(44) Huo, S.; Wang, J.; Cieplak, P.; Kollman, P. A.; Kuntz, I. D. Molecular dynamics and free energy analyses of cathepsin D-inhibitor interactions: insight into structure-based ligand design. *J. Med. Chem.* **2002**, *45*, 1412−1419.
(45) Tuccinardi, T.; Bertini, S.; Martinelli, A.; Minutolo, F.; Ortore, G.; Placanica, G.; Prota, G.; Rapposelli, S.; Carlson, K. E.; Katzenellenbogen, J. A.; Macchia, M. Synthesis of anthranylaldoxime derivatives as estrogen receptor ligands and computational prediction of binding modes. *J. Med. Chem.* **2006**, *49*, 5001−5012.
(46) Knowles, P. P.; Murray-Rust, J.; Kjaer, S.; Scott, R. P.; Hanrahan, S.; Santoro, M.; Ibanez, C. F.; McDonald, N. C. Structure and chemical inhibition of the RET tyrosine kinase domain. *J. Biol. Chem.* **2006**, *281*, 33577−33587.
(47) Cuccuru, G.; Lanzi, C.; Cassinelli, G.; Pratesi, G.; Tortoreto, M.; Petrangolini, G.; Seregni, E.; Martinetti, A.; Laccabue, D.; Zanchi, C.; Zunino, F. Cellular effects and antitumor activity of RET inhibitor RPI-1 on MEN2A-associated medullary thyroid carcinoma. *J. Natl. Cancer. Inst.* **2004**, *96*, 1006−1014.
(48) Gasteiger, E.; Gattiker, A.; Hoogland, C.; Ivanyi, I.; Appel, R. D.; Bairoch, A. ExPASy: The proteomics server for in-depth protein knowledge and analysis. *Nucleic Acids Res.* **2003**, *31*, 3784−3788.
(49) Altschul, S. F.; Madden, T. L.; Schäffer, A. A.; Zhang, J.; Zhang, Z.; Miller, W.; Lipman, D. J. Gapped BLAST and PSI-BLAST: a new generation of protein database search programs. *Nucleic Acids Res.* **1997**, *25*, 3389−3402.
(50) Berman, H. M.; Westbrook, J.; Feng, Z.; Gilliland, G.; Bhat, T. N.; Weissig, H.; Shindyalov, I. N.; Bourne, P. E. The Protein Data Bank. *Nucl. Acids Res.* **2000**, *28*, 235−242.
(51) Thompson, J. D.; Higgins, D. G.; Gibson, T. J. CLUSTAL W: improving the sensitivity of progressive multiple sequence alignment through sequence weighting, position-specific gap penalties and weight matrix choice. *Nucleic Acids Res.* **1994**, *22*, 4673−4680.
(52) Case, D. A.; Darden, T. A.; Cheatham, T. E., III; Simmerling, C. L.; Wang, J.; Duke, R. E.; Luo, R.; Merz, K. M.; Wang, B.; Pearlman, D. A.; Crowley, M.; Brozell, S.; Tsui, V.; Gohlke, H.; Mongan, J.; Hornak, V.; Cui, G.; Beroza, P.; Schafmeister, C.; Caldwell, J. W.; Ross, W. S.; Kollman, P. A. *AMBER 8*; University of California: San Francisco, CA, 2004.
(53) *Macromodel, version 8.5*; Schrödinger Inc.: Portland, OR, 1999.
(54) Coon, S. Overview of the AutoTools suite. http://www.scripps.edu/~sanner/python/adt (accessed February 2001).
(55) Walker, R. Tutorial B1. http://amber.scripps.edu/tutorials/basic/tutorial1 (accessed 2004).
(56) Pastor, R. W.; Brooks, B. R.; Szabo, A. An analysis of the accuracy of Langevin and molecular dynamics algorithms. *Mol. Phys.* **1988**, *65*, 1409−1419.
(57) Loncharich, R. J.; Brooks, B. R.; Pastor, R. W. Langevin dynamics of peptides: The frictional dependence of isomerization rates of *N*-actylananyl-*N*′-methylamide. *Biopolymers* **1992**, *32*, 523−535.

CI6004383